

Fusion Imaging to Guide Thoracic Endovascular Aortic Repair (TEVAR): A Randomized Comparison of Two Methods, 2D/3D Versus 3D/3D Image Fusion

P.-A. Barral^{1,2} · M. A. Demasi-Jacquier^{2,3} · L. Bal^{2,3} · V. Omnes^{2,3} · A. Bartoli^{1,2} · P. Piquet^{2,3} · A. Jacquier^{1,2} · M. Gaudry^{2,3}

Received: 11 April 2019 / Accepted: 30 July 2019 / Published online: 3 September 2019
© Springer Science+Business Media, LLC, part of Springer Nature and the Cardiovascular and Interventional Radiological Society of Europe (CIRSE) 2019

Abstract

Purpose To compare the accuracy of two-dimensional (2D) versus three-dimensional (3D) image fusion for thoracic endovascular aortic repair (TEVAR) image guidance. **Materials and Methods** Between December 2016 and March 2018, all eligible patients who underwent TEVAR were prospectively included in a single-center study. Image fusion methods (2D/3D or 3D/3D) were randomly assigned to guide each TEVAR and compared in terms of accuracy,

dose area product (DAP), volume of contrast medium injected, fluoroscopy time and procedure time.

Results Thirty-two patients were prospectively included; 18 underwent 2D/3D and 14 underwent 3D/3D TEVAR. The 3D/3D method allowed more accurate positioning of the aortic mask on top of the fluoroscopic images (proximal landing zone error vector: 1.7 ± 3.3 mm) than was achieved by the 2D/3D method (6.1 ± 6.1 mm; $p = 0.03$). The 3D/3D image fusion method was associated with significantly lower DAP than the 2D/3D method (50.5 ± 30.1 Gy cm² for 3D/3D vs. 99.5 ± 79.1 Gy cm² for 2D/3D; $p = 0.03$). The volume of contrast medium injected was significantly lower for the 3D/3D method than for the 2D/3D method (50.6 ± 22.9 ml vs. 98.4 ± 47.9 ml; $p = 0.002$).

Conclusion Higher image fusion accuracy and lower contrast volume and irradiation dose were observed for 3D/3D image fusion than for 2D/3D during TEVAR.

Level of Evidence II, Randomized trial.

✉ P.-A. Barral
Pierre-Antoine.BARRAL@ap-hm.fr

M. A. Demasi-Jacquier
Mariangela.DEMASI@ap-hm.fr

L. Bal
Laurence.BAL@ap-hm.fr

V. Omnes
Virgile.OMNES@ap-hm.fr

A. Bartoli
Axel.BARTOLI@ap-hm.fr

P. Piquet
Phillipe.PIQUET@ap-hm.fr

A. Jacquier
Alexis.JACQUIER@ap-hm.fr

M. Gaudry
Marine.GAUDRY@ap-hm.fr

Keywords Aorta · Thoracic · Endovascular procedures · Multimodal imaging · Radiation protection

Introduction

Thoracic endovascular aortic repair (TEVAR) has been recognized as the first-line treatment for descending thoracic aorta aneurysms and is now considered the preferred treatment for complicated type B dissection [1–5]. The

¹ Centre Aorte Timone, Hôpital de la Timone, 264 rue saint Pierre, 13385 Marseille Cedex 05, France

² Department of Radiology, Hôpital de la Timone, 264 rue saint Pierre, 13385 Marseille Cedex 05, France

³ Department of Vascular Surgery, Hôpital de la Timone, 264 rue saint Pierre, 13385 Marseille Cedex 05, France

safety and accuracy of the procedure [6] are the main reasons for the development of fusion imaging. Modern fixed flat-panel detectors have been demonstrated to have a higher imaging performance than that of two-dimensional (2D) fluoroscopy imaging systems (mobile C-arms) [7]. Dramatic progress has been made in computer power and software, allowing preoperative computed tomography angiography (CTA) to be combined with fluoroscopy or cone beam computed tomography (CBCT) acquisition to obtain 3D vascular roadmaps of the aorta and visceral vessels that can be displayed on top of live fluoroscopic images. Fusion imaging has been shown to drive contrast volume and irradiation reductions during endovascular aortic repair (EVAR) [8–12].

There are two ways to perform image fusion: the first generation of image fusion was the 2D/3D method, which uses bone landmarks on fluoroscopy to register the two modalities. The second generation was the 3D/3D method, which uses remarkable landmarks on a noncontrast CBCT (nCBCT) to register the two modalities. Both 2D/3D and 3D/3D methods have been evaluated in EVAR [12]. The accuracy of 3D/3D registration in EVAR was measured and found to be approximately 5 mm in the craniocaudal direction with an absolute deviation of approximately 5 mm

No clear comparison among available fusion methods has been published to guide TEVAR.

Our hypothesis is that the 3D/3D method is more accurate than the 2D/3D method for guiding TEVAR. The aim of the present study was to randomly compare 2D/3D versus 3D/3D image fusion for TEVAR image guidance in terms of anatomic accuracy, dose area product (DAP), quantity of contrast medium injected and fluoroscopy time.

Materials and Methods

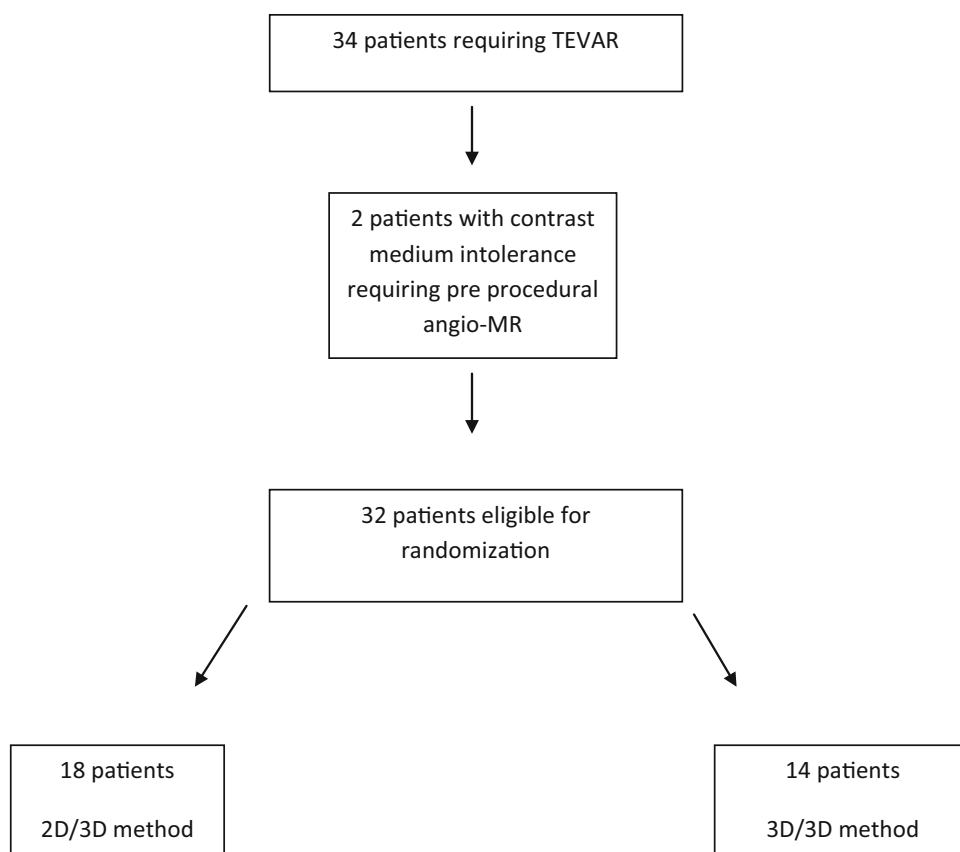
All eligible patients referred for a thoracic aortic lesion requiring TEVAR between December 2016 and March 2018 were prospectively included in this single-center study (Fig. 1). The study was approved by the local ethics committee, and all patients gave their informed consent. The inclusion criteria were as follows: patients with a thoracic aortic lesion, including aneurysm, false aneurysm, type B aortic dissection, penetrating aortic ulcer (PAU) and endoleak, which required TEVAR based on the current recommendations for best medical practice [1, 4] and the decision of a multidisciplinary team comprising vascular surgeons, radiologists, cardiologists and anesthesiologists; and CTA within 1 month before the procedure. Patients requiring open surgery or emergency treatment were not included. Patients with contraindications to iodine injection were excluded. All eligible patients were randomized for

either 2D/3D or 3D/3D image fusion to guide the TEVAR procedure based on random draws the day of the TEVAR. The primary end point was image fusion error, which was defined as the maximal distance (Euclidean 2D distance) between the same remarkable anatomic landmarks on the vascular subvolume and on the first digital subtraction angiography (DSA-run) in the proximal landing zone in the selected working incidence (expressed in millimeters) (Fig. 2). Complete accuracy was defined as a lack of discrepancy between the mask position and the thoracic aorta position during the first DSA-run. Secondary end points were image fusion error at the distal neck (expressed in millimeters), quantification of the DAP (expressed in Gy cm²), including noncontrast acquisition to build 2D/3D and 3D/3D masks, volume of contrast medium injected (expressed in milliliters) and fluoroscopy time (expressed in minutes); endovascular time was defined as the delay between the first and the last fluoroscopy. All patients underwent preprocedural CTA (Revolution EVO or Optima 660, GE Healthcare, Chicago, USA). CTA scans were performed after the administration of a bolus of 1 cc/kg of a nonionic contrast medium flushed with a bolus of 30 cc of a saline solution. The acquisition parameters were as follows: slice thickness = 0.6 mm; pitch = 1.3; reconstruction slice thickness = 0.6 mm; peak voltage = 120 kV; and automatic modulation of mAs. All TEVAR procedures were performed under general anesthesia using the same angiographic system equipped with 3D angiography (Discovery IGS 730, GE Healthcare). Pulsed fluoroscopy was 15 pulses per second, and the DSA-run was 2 frames per second. We used commercially available software that allowed 2D/3D and 3D/3D image fusion with preprocedural CTA (AW server 4.7 GE Healthcare). TEVAR was considered successful if the lesion was excluded on the last DSA-run. The same operator carried out the image fusion for 2D/3D and 3D/3D during the inclusion period after completing a training program by GE Healthcare. The team performing the procedures included two vascular surgeons and two interventional radiologists. In-room acquisitions required to build 2D/3D or 3D/3D fusion were performed before sterile draping to preserve asepsis and save time. Fusion processes were performed during patient preparation for surgery after general anesthesia.

2D/3D Image Fusion Workflow (Fig. 3)

The preoperative CTA was first segmented into two subvolumes for the vascular tree and bone structures in volume rendering by automatic or manual segmentation. Subvolumes were defined by volume rendering reconstruction exclusively showing the vascular tree or bone structures. Segmented volumes were then exported to a workstation in

Fig. 1 Flowchart. Two patients were excluded because of contrast media intolerance. Sixteen patients were randomized to the 3D/3D group, and 18 patients were randomized to the 2D/3D group



the angiography room. The bone subvolume was first superimposed onto two fluoroscopic orthogonal incidences (anteroposterior and lateral) and aligned using the position of the vertebrae and ribs. When the alignment between the CTA and the two fluoroscopic orthogonal angles was considered to be the best achievable, the image fusion was validated. The bone subvolume was then replaced by the vascular subvolume.

3D/3D Workflow (Fig. 4)

A nCBCT was acquired and centered on the aortic lesion. In contrast to 2D/3D fusion imaging, anatomical landmarks, such as calcifications, surgical clips, or vessel bifurcations, visible on both nCBCT and preoperative CTA and as close as possible to the landing zone, were used to register the two modalities. The 3D/3D image fusion was performed using a dedicated software (Fusion RX IRM, AW, GE Healthcare) and validated until the image fusion was judged to be the best achievable. The vascular subvolume segmented from the preoperative CTA was then overlaid onto the live fluoroscopic image.

In both cases, it was possible to make fine adjustments to the mask during the course of the procedure using DSA-run. The position of the vascular subvolume was adjusted to obtain a perfect fit with the vascular subvolume and the

thoracic aorta on DSA-run. During the hospital stay, creatinine was recorded for each patient.

Statistical Analysis

Continuous variables are expressed as the mean \pm standard deviation. The required sample size was estimated to be 26 patients under the following hypotheses: (1) an expected mean bias between DSA-run and 2D/3D of 6 mm, (2) a mean bias between DSA-run and 3D/3D of 2 mm, (3) a standard deviation of 2 mm based on our experience, (4) a balanced randomization ratio (1:1) between 2D/3D and 3D/3D, (5) a bilateral alpha risk of 0.05, and (6) a beta risk of 0.10 (i.e., a power of 0.90). This sample size was increased to 32 to account for potential technical difficulties or imbalanced randomization due to block randomization with a random block size from 2 to 6. The distribution of variables was assessed using the Kolmogorov–Smirnov test. Categorical variables are presented as absolute terms and percentages. Categorical variables were compared with Chi-squared tests, and continuous variables were compared with Student's *t* test. A *p* value less than .05 was considered to be statistically significant. Statistical analyses were performed using GraphPad Statistics (GraphPad Software, Inc., San Diego, USA).



Fig. 2 Image fusion error between the aortic wall contour on the vascular subvolume and the DSA-run in the proximal landing zone (double white arrow: ostium of the left common carotid artery). Note the carotid-subclavian bypass (white star)

Results

Thirty-four patients were prospectively included, and TEVAR was successful in all cases. Two patients were excluded because of contrast medium intolerance. The patient characteristics are summarized in Table 1. All 2D/3D and 3D/3D fusion images were performed during in-room patient preparation without any delay of the intervention. Eighteen patients were assigned to 2D/3D and 14 were assigned to the 3D/3D fusion imaging method. Image fusion errors in the proximal landing zone were significantly lower for 3D/3D (1.7 ± 3.3 mm) than for 2D/3D (6.1 ± 6.1 mm; $p = 0.03$). The results were similar for the distal landing zone, where the fusion error was measured at 1.3 ± 0.5 mm for 3D/3D versus 7.5 ± 7.3 mm for 2D/3D ($p = 0.008$). No significant difference was observed between proximal and distal landing zone errors for either 3D/3D or 2D/3D (Table 2, Fig. 5). Complete accuracy was obtained in 7/14 patients with 3D/3D image fusion but was never obtained in the 2D/3D image fusion group. There was no significant difference in fluoroscopy time between the 3D/3D and 2D/3D image fusion groups (17.0 ± 7.4 min and 19.2 ± 6.8 min, respectively, $p = 0.3$). In contrast, DAP and contrast volume were lower

for 3D/3D image fusion than for 2D/3D image fusion (50.5 ± 30.1 Gy.cm² vs. 99.5 ± 79.2 ; $p = 0.03$ and 50.6 ± 22.9 ml vs. 98.4 ± 47.9 ; $p = 0.002$) (Figs. 6, 7; Table 3). The nCBCT radiation dose was included in the DAP of the 3D/3D group and was $DAP = 1.7 \pm 0.6$ Gy cm². The orthogonal fluoroscopic incidence dose was $DAP = 0.1 \pm 0.05$ Gy cm². The DSA-run required during 2D/3D was 6.8 ± 0.8 higher compared to 3D/3D (4.0 ± 0.2 ; $p = 0.007$). Endovascular time was not significantly shorter when performed using 3D/3D image fusion (123.1 ± 53.6 min vs. 113.7 ± 17.5 min, $p = 0.5$) (Table 3). There was no progression of the aneurysm or the diameter of the false lumen at 1 month after TEVAR in either group. No significant modification of renal function was measured during the hospital stay or at a 1-month follow-up.

Discussion

We found that 3D/3D image fusion was a more accurate image fusion method when used to guide TEVAR procedures, and compared to the 2D/3D method, the 3D/3D method reduced the irradiation dose and the quantity of contrast medium. The causes of image fusion inaccuracy are multiple: preoperative CTs are usually performed with the arms in an upward position, while TEVAR is usually performed with the patient in the arms-down position. This difference may partially explain why 3D/3D performed better than 2D/3D. 3D/3D image fusion is based on aortic anatomical landmarks and not bony landmarks. When using 2D/3D settings, the anatomical landmarks are selected on the spine and bones, increasing the anatomical aortic bias between the two examinations. Another explanation for the image fusion inaccuracy of both 2D/3D and 3D/3D is the introduction of rigid materials, such as stiff guidewires, introducer sheaths and undeployed stent grafts, into the lumen of the vessel, resulting in the significant deformation and straightening of the abdominal aorta [13]. In the abdominal section, the motion of the aortic and iliac centerline during EVAR is significant: Kaladji et al. [13] assessed this movement to be approximately 1.5 ± 0.4 mm and associated with aortic neck angulation ($> 30^\circ$). The motion of the lowest renal artery during EVAR was assessed by Kaufmann et al. [14] to be approximately 10.6 mm in axial plane and 7.4 mm in the z-axis.

This well-known discrepancy between sub-volume position and anatomical aortic position during an endovascular procedure for EVAR explains why the recommended workflow for EVAR is to adjust the mask with a DSA-run at the renal level after the introduction of an undeployed stent graft. Subsequently, the image fusion method before adjustment with DSA does not need to be

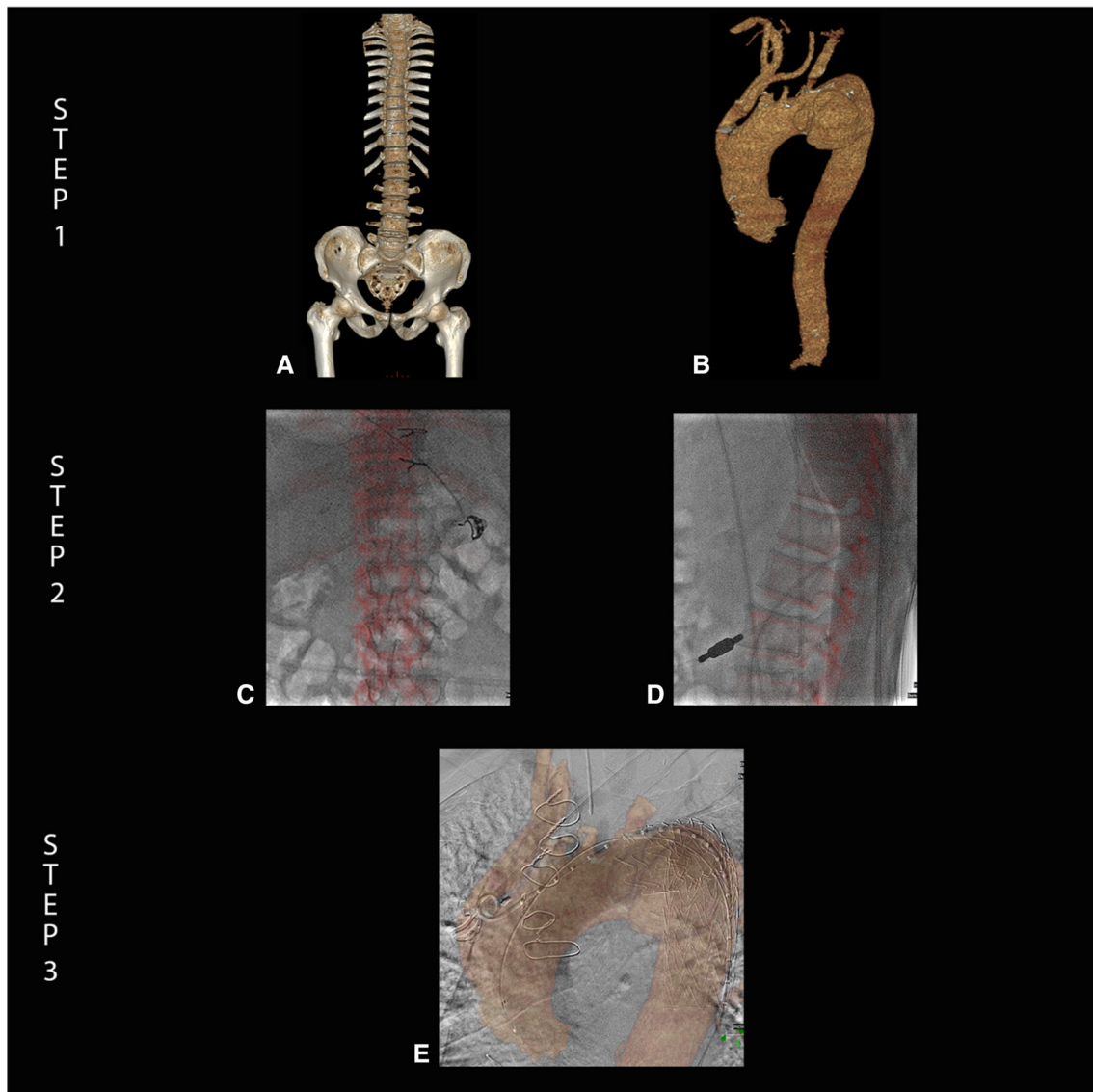


Fig. 3 Workflow for 2D/3D image fusion. Step 1: extraction of bone (A) and vascular (B) volume from the same preoperative CTA. Step 2: image fusion using two orthogonal fluoroscopic incidences: the objective of this step is to merge the bone mask (shown in red in C and D) and bone structure on the fluoroscopy in a frontal view

(c) and a lateral view (D). Note that a significant gap between mask and fluoroscopy was left for didactic reasons. Step 3: when the mask and fluoroscopic view matched perfectly, the bone mask was switched off, and the vascular volume was switched on and used as a 3D road map overlaying the fluoroscopic image

accurate at the abdominal aortic level due to vessel deformation during endovascular navigation. In the present study, the accuracy of the 3D/3D image fusion method suggests that subtle deformations of the thoracic aorta were related to the presence of the wire and the stent graft [15]. In the thoracic aorta, the presented results suggest that the main cause of image fusion misregistration when using the 2D/3D method was anatomical bias between anatomical landmarks selected on the spine and bones and the aortic location. The 3D/3D fusion method, which is based on aortic anatomical landmarks, removes the bias caused by the relative displacement between the bone and aorta.

Furthermore, Barral et al. [16] recently showed that the use of DSA-run to adjust the image fusion subvolume may not be mandatory for TEVAR if the 3D/3D method is used. Goudekette and Ahmad [17, 18] found that the use of fusion imaging was associated with a significant reduction in the volume of contrast injected during endovascular aortic repair without distinction between 2D/3D and 3D/3D fusion.

Lessard et al. [19] showed that a wire inserted in the aortic lumen could be automatically detected and used to adapt a nonrigid image fusion method. This technique could contribute to further reducing the contrast medium

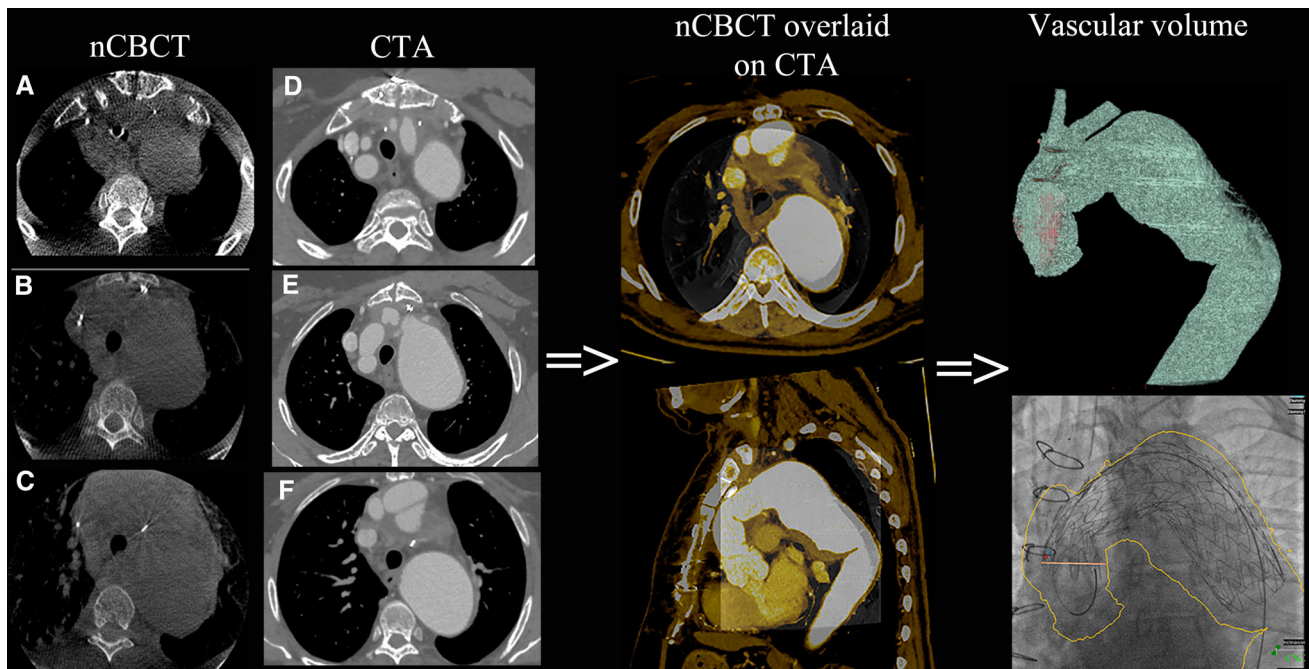


Fig. 4 Workflow for 3D/3D image fusion. The first step was to select the same anatomic landmarks on nCBCT and CTA. In the presented case, three surgical clips placed at different levels of the aortic arch were selected as remarkable landmarks assessable on both nCBCT and CTA (arrows in **A** and **D** show the first landmark, arrows in **B** and **E** show the second, and arrows in **C** and **F** show the third). After merging the three landmarks, the software proposed a manual correction of the mask position over nCBCT. For that step, nCBCT was overlaid on the CTA in axial view, and in the sagittal oblique

view, the position of the vascular mask on CTA could be adapted to better match the aortic position on nCBCT. When the vascular mask and the actual position of the aorta were merged, the vascular mask was overlaid on the fluoroscopic image and used as a 3D roadmap. Note that the orthogonal ring (white arrow) and dot (white arrowhead) were drawn on the vascular mask and used to precisely locate the proximal aortic neck and ostium of the supra-aortic trunk transposition

Table 1 Patient data and type of aortic disease

	2D/3D image fusion (n = 18)	3D/3D image fusion (n = 14)
Age (years)	65 ± 14.9	67 ± 13.8
Male sex: n (%)	14 (78)	13 (81)
BMI (kg/m ²)	25.1 ± 4.5	26.4 ± 4.4
Aneurysm/false aneurysm: n (%)	2 (11.1)	5 (31.2)
Aortic dissection: n (%)	6 (33.3)	7 (43)
Endoleak: n (%)	3 (16.6)	0
PAU: n (%)	7 (38.8)	4 (25)

BMI body mass index, PAU penetrating aortic ulcer

Table 2 Fusion imaging accuracy

	Deviation between vascular volume and DSA-run		p values
	Proximal landing zone (mm)	Distal landing zone (mm)	
2D/3D image fusion	6.1 ± 6.1	7.5 ± 7.3	0.6
3D/3D image fusion	1.7 ± 3.3	1.3 ± 0.5	0.7
p values	0.03	0.008	

Values are presented as the mean ± standard deviation

volume and DAP [13, 19]. Even though nCBCT gives more irradiation (DAP = 1.7 Gy cm²) than two fluoroscopy orthogonal incidences (DAP = 0.1 Gy cm²), the difference

in DAP could be explained by the higher number of DSA-runs required during 2D/3D fusion to adapt the position of the mask during imaging guidance. Furthermore, the

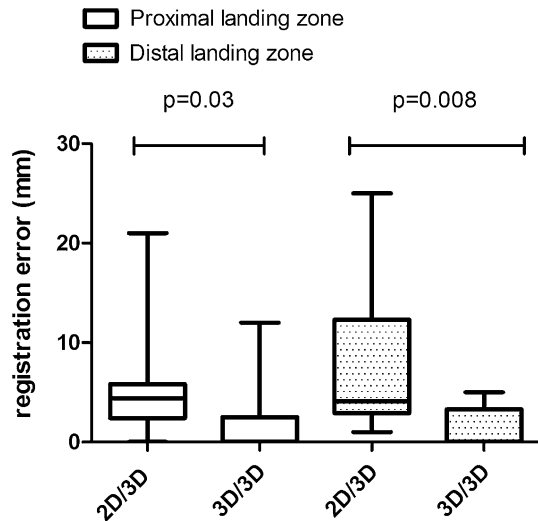


Fig. 5 Image fusion error in the proximal and distal landing zones with 2D/3D and 3D/3D image fusion

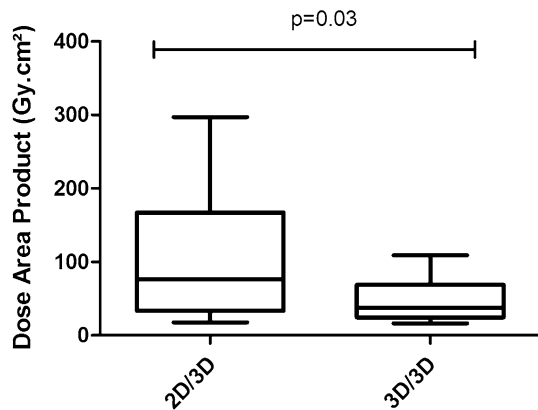


Fig. 6 Dosimetry during TEVAR with 2D/3D image fusion and 3D/3D image fusion

nCBCT irradiation is distributed circumferentially over 200° on the patient. In the present study, the reported mean DAP was comparable with data already published in the literature, ranging from 90.4 Gy cm² (61.9–158.5), as published by Dias et al. [20], to 26.1 Gy cm² (11.9–34.9), as published by Hertault et al. [20]. Two studies reported higher mean DAP values of 324.2 Gy cm² (41.7–789.1) in

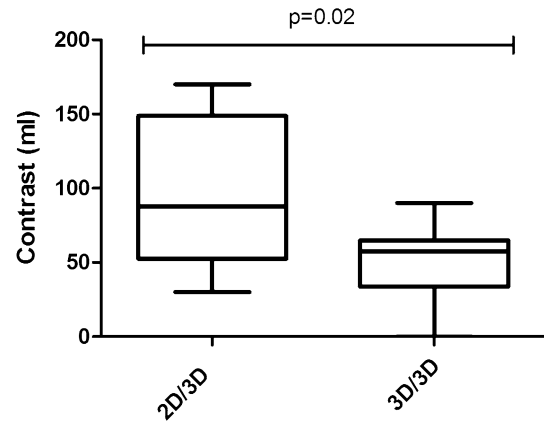


Fig. 7 Contrast volume used during TEVAR with 2D/3D image fusion and 3D/3D image fusion

Schultz et al. [21] and 194.4 Gy cm² (112.84–351.01) in Howells et al. [22]. These heterogeneous results could be due to the type of angiographic suite used and differences in medical practice. The amount of contrast volume injected in the current series is comparable with the published data described in the literature [10, 18, 20–23].

Study Limitations

The limited field of view (23 × 23 cm) of nCBCT represents a limit of this technique. In the study settings, the vascular mask used for 3D/3D fusion could not be larger than the nCBCT field of view. This constraint might limit the use of 3D/3D fusion if several sites of the aorta have to be treated. This study is a nonblinded study, and all efforts to produce quality research may have been limited by this bias. Another limitation of this study is that we did not use the same alignment structures (i.e., bony landmarks, which would have been possible) in 2D/3D and 3D/3D.

The significance of the impact on patient prognosis was not evaluated in the present report, as it was not within the scope of the study. Further larger studies are required to determine whether the use of fusion could have an impact on patient prognosis.

Table 3 Radiation exposure, contrast volume and procedure time

	Dosimetry		Contrast medium volume (ml)	Endovascular time (min)
	Fluoroscopy time (min)	DAP (Gy cm ²)		
2D/3D image fusion	19.2 ± 6.8	99.5 ± 79.2	98.4 ± 47.9	123.1 ± 53.6
3D/3D image fusion	17.0 ± 7.4	50.5 ± 30.1	50.6 ± 22.9	113.7 ± 17.5
<i>p</i> values	0.3	0.03	0.002	0.5

Values are presented as mean ± standard deviation

DAP dose area product

Conclusion

The 3D/3D image fusion technique yielded higher image fusion accuracy and lower contrast volume and irradiation dose than was achieved by 2D/3D during TEVAR.

Funding This study was not supported by any funding.

Compliance with Ethical Standards

Conflict of interest The authors declare that they have no conflict of interest.

Human and Animal Rights All procedures performed in studies involving human participants were in accordance with the ethical standards of the institutional and/or national research committee and with the 1964 Helsinki declaration and its later amendments or comparable ethical standards.

Informed Consent Informed consent was obtained from all individual participants included in the study.

Consent for Publication Consent for publication was obtained for every individual person's data included in the study.

References

1. ESC Guidelines on the diagnosis and treatment of aortic diseases: document covering acute and chronic aortic diseases of the thoracic and abdominal aorta of the adult. The task force for the diagnosis and treatment of aortic diseases of the European Society of Cardiology (ESC). *Eur Heart J* 2014;35(41):2873–926.
2. Evangelista A, Czerny M, Nienaber C, Schepens M, Rousseau H, Cao P, et al. Interdisciplinary expert consensus on management of type B intramural haematoma and penetrating aortic ulcer. *Eur J Cardio Thorac Surg*. 2015;47(2):209–17.
3. Dake MD, Kato N, Mitchell RS, Semba CP, Razavi MK, Shimono T, et al. Endovascular stent-graft placement for the treatment of acute aortic dissection. *N Engl J Med*. 1999;340(20):1546–52.
4. Grabenwoger M, Alfonso F, Bachet J, Bonser R, Czerny M, Eggebrecht H, et al. Thoracic Endovascular Aortic Repair (TEVAR) for the treatment of aortic diseases: a position statement from the European Association for Cardio-Thoracic Surgery (EACTS) and the European Society of Cardiology (ESC), in collaboration with the European Association of Percutaneous Cardiovascular Interventions (EAPCI). *Eur J Cardio Thorac Surg*. 2012;42(1):17–24.
5. Nauta FJ, Trimarchi S, Kamman AV, Moll FL. Update in the management of type B aortic dissection. *Vasc Med*. 2016;21(3):251–63.
6. Koutouzi G, Sandström C, Roos H, Henrikson O, Leonhardt H, Falkenberg M. Orthogonal rings, fiducial markers, and overlay accuracy when image fusion is used for EVAR guidance. *Eur J Vasc Endovasc Surg*. 2016;52(5):604–11.
7. Panayotopoulos P, Bouvier A, Besnier L, Rousselet MC, Nedelcu C, Baize N, et al. Laparoscopic partial nephrectomy following tumor embolization in a hybrid room. Feasibility and clinical outcomes. *Surg Oncol*. 2017;26(4):377–81.
8. Koutouzi G, Henrikson O, Roos H, Zachrisson K, Falkenberg M. EVAR guided by 3D image fusion and CO₂ DSA: a new imaging combination for patients with renal insufficiency. *J Endovasc Ther*. 2015;22(6):912–7.
9. Kaladji A, Dumenil A, Mahé G, Castro M, Cardon A, Lucas A, et al. Safety and accuracy of endovascular aneurysm repair without pre-operative and intra-operative contrast agent. *Eur J Vasc Endovasc Surg*. 2015;49(3):255–61.
10. Hertault A, Maurel B, Sobocinski J, Martin Gonzalez T, Le Roux M, Azzaoui R, et al. Impact of hybrid rooms with image fusion on radiation exposure during endovascular aortic repair. *Eur J Vasc Endovasc Surg*. 2014;48(4):382–90.
11. Kobeiter H, Nahum J, Becquemin J-P. Zero-contrast thoracic endovascular aortic repair using image fusion. *Circulation*. 2011;124(11):e280–2.
12. Tacher V, Lin M, Desgranges P, Deux J-F, Grünhagen T, Becquemin J-P, et al. Image guidance for endovascular repair of complex aortic aneurysms: comparison of two-dimensional and three-dimensional angiography and image fusion. *J Vasc Interv Radiol*. 2013;24(11):1698–706.
13. Kaladji A, Dumenil A, Castro M, Cardon A, Becquemin J-P, Bou-Saïd B, et al. Prediction of deformations during endovascular aortic aneurysm repair using finite element simulation. *Comput Med Imaging Graph*. 2013;37(2):142–9.
14. Kauffmann C, Douane F, Therasse E, Lessard S, Elkouri S, Gilbert P, et al. Source of errors and accuracy of a two-dimensional/three-dimensional fusion road map for endovascular aneurysm repair of abdominal aortic aneurysm. *J Vasc Interv Radiol*. 2015;26(4):544–51.
15. Carrell TW, Modarai B, Brown JR, Penney GP. Feasibility and limitations of an automated 2D-3D rigid image registration system for complex endovascular aortic procedures. *J Endovasc Ther*. 2010;17(4):527–33.
16. Barral P-A, De Masi-Jacquier M, Gaudry M, Boutboul D, Bartoli J-M, Jacquier A, et al. Three-dimensional to three-dimensional image fusion-guided thoracic endovascular aortic repair without iodine injection. *J Vasc Interv Radiol*. 2017;28(8):1201–3.
17. Goudekettig SR, Heinen SGH, Ünli Ç, van den Heuvel DAF, de Vries J-PPM, van Strijen MJ, et al. Pros and Cons of 3D image fusion in endovascular aortic repair: a systematic review and meta-analysis. *J Endovasc Ther*. 2017;24(4):595–603.
18. Ahmad W. Image fusion using the two-dimensional-three-dimensional registration method helps reduce contrast medium volume, fluoroscopy time, and procedure time in hybrid thoracic endovascular aortic repairs. *J Vasc Surg*. 2018;8:1003–10.
19. Lessard S, Kauffmann C, Pfister M, Cloutier G, Thérèse É, de Guise JA, et al. Automatic detection of selective arterial devices for advanced visualization during abdominal aortic aneurysm endovascular repair. *Med Eng Phys*. 2015;37(10):979–86.
20. Dias NV, Billberg H, Sonesson B, Törnqvist P, Resch T, Kristmundsson T. The effects of combining fusion imaging, low-frequency pulsed fluoroscopy, and low-concentration contrast agent during endovascular aneurysm repair. *J Vasc Surg*. 2016;63(5):1147–55.
21. Schulz CJ, Schmitt M, Böckler D, Geisbüsch P. Feasibility and accuracy of fusion imaging during thoracic endovascular aortic repair. *J Vasc Surg*. 2016;63(2):314–22.
22. Howells P, Eaton R, Patel AS, Taylor P, Modarai B. Risk of radiation exposure during endovascular aortic repair. *Eur J Vasc Endovasc Surg*. 2012;43(4):393–7.
23. Zoli S, Trabattini P, Dainese L, Annoni A, Saccu C, Fumagalli M, et al. Cumulative radiation exposure during thoracic endovascular aneurysm repair and subsequent follow-up. *Eur J Cardio Thorac Surg*. 2012;42(2):254–60.

Publisher's Note Springer Nature remains neutral with regard to jurisdictional claims in published maps and institutional affiliations.